The dependence of dark matter profiles on the stellar-to-halo mass ratio: a prediction for cusps versus cores

Arianna Di Cintio,[1,2]⋆ Chris B. Brook,[1] Andrea V. Macciò,[3] Greg S. Stinson,[3] Alexander Knebe,[1] Aaron A. Dutton[3] and James Wadsley[4]

[1]*Departamento de Física Teórica, Módulo C-15, Facultad de Ciencias, Universidad Autónoma de Madrid, E-28049 Cantoblanco, Madrid, Spain*
[2]*Physics Department G. Marconi, Università di Roma Sapienza, Ple Aldo Moro 2, I-00185 Rome, Italy*
[3]*Max-Planck-Institut für Astronomie, Königstuhl 17, D-69117 Heidelberg, Germany*
[4]*McMaster University, Hamilton, ON L8S 4M1, Canada*

ABSTRACT

We use a suite of 31 simulated galaxies drawn from the MaGICC project to investigate the effects of baryonic feedback on the density profiles of dark matter haloes. The sample covers a wide mass range: $9.4 \times 10^9 < M_{halo}/M_\odot < 7.8 \times 10^{11}$, hosting galaxies with stellar masses in the range $5.0 \times 10^5 < M_*/M_\odot < 8.3 \times 10^{10}$, i.e. from dwarf to L*. The galaxies are simulated with blastwave supernova feedback and, for some of them, an additional source of energy from massive stars is included. Within this feedback scheme we vary several parameters, such as the initial mass function, the density threshold for star formation, and energy from supernovae and massive stars. The main result is a clear dependence of the inner slope of the dark matter density profile, α in $\rho \propto r^\alpha$, on the stellar-to-halo mass ratio, M_*/M_{halo}. This relation is independent of the particular choice of parameters within our stellar feedback scheme, allowing a prediction for cusp versus core formation. When M_*/M_{halo} is low, $\lesssim 0.01$ per cent, energy from stellar feedback is insufficient to significantly alter the inner dark matter density, and the galaxy retains a cuspy profile. At higher stellar-to-halo mass ratios, feedback drives the expansion of the dark matter and generates cored profiles. The flattest profiles form where $M_*/M_{halo} \sim 0.5$ per cent. Above this ratio, stars formed in the central regions deepen the gravitational potential enough to oppose the supernova-driven expansion process, resulting in cuspier profiles. Combining the dependence of α on M_*/M_{halo} with the empirical abundance matching relation between M_* and M_{halo} provides a prediction for how α varies as a function of stellar mass. Further, using the Tully–Fisher relation allows a prediction for the dependence of the dark matter inner slope on the observed rotation velocity of galaxies. The most cored galaxies are expected to have $V_{rot} \sim 50\,km\,s^{-1}$, with α decreasing for more massive disc galaxies: spirals with $V_{rot} \sim 150\,km\,s^{-1}$ have central slopes $\alpha \le -0.8$, approaching again the Navarro–Frenk–White profile. This novel prediction for the dependence of α on disc galaxy mass can be tested using observational data sets and can be applied to theoretical modelling of mass profiles and populations of disc galaxies.

Key words: hydrodynamics – galaxies: evolution – galaxies: formation – dark matter.

1 INTRODUCTION

The Λ cold dark matter (ΛCDM) cosmological model has been shown to agree with observations of structures on large scales [e.g. Riess et al. 1998; Komatsu et al. 2011; Ade et al. (Planck Collaboration) 2013; Hinshaw et al. 2013]. According to this theory, galaxies

are embedded within DM haloes (White & Rees 1978; Blumenthal et al. 1984), whose properties have been extensively studied in the past, thanks to numerical *N*-body simulations (e.g. Springel 2005; Power & Knebe 2006; Macciò, Dutton & van den Bosch 2008; Kuhlen, Vogelsberger & Angulo 2012). Problems at small scales, however, still affect the ΛCDM model, one of which is the so-called 'cusp-core' problem. A prediction of pure DM collisionless simulations is that DM density increases as $\rho \propto r^{-1}$ towards the halo centre (Navarro, Frenk & WhiteNavarro et al. 1996b; Springel et al.

⋆ E-mail: arianna.dicintio@uam.es

2008; Navarro et al. 2010). The existence of such a 'cuspy' density profile is in disagreement with observations of disc and dwarf galaxies (e.g. Salucci & Burkert 2000; Simon et al. 2005; de Blok et al. 2008; Kuzio de Naray, McGaugh & de Blok 2008; Kuzio de Naray, McGaugh & Mihos 2009; Oh et al. 2011), where detailed mass modelling using rotation curves suggests a flatter, or 'cored', DM density profile. Simulated DM haloes modelled with an Einasto (Einasto 1965) profile have an inner slope of -0.7 (Graham et al. 2006): this value is closer to what observed in real galaxies (Swaters et al. 2003), yet not sufficient to solve the discrepancy (de Blok, Bosma & McGaugh 2003).

One possibility, without resorting to more exotic forms of DM (e.g. warm DM, see Avila-Reese et al. 2001; Bode, Ostriker & Turok 2001; Knebe et al. 2002; Macciò et al. 2012b), is that this inconsistency arises from having neglected the effects of baryons, which are irrelevant on cosmological scales where DM and dark energy dominate, but may be dynamically relevant on small, galactic scales. For example, as gas cools to the central region of galaxy haloes, it adiabatically contracts DM to the centre (e.g. Blumenthal et al. 1986; Gnedin et al. 2004). Such adiabatic contraction exacerbates the mismatch between the profiles of DM haloes and the observed density profiles inferred from rotation curves. Further, theoretical models with halo contraction are unable to self-consistently reconcile the observed galaxy scaling relations, such as the rotation velocity–luminosity and size–luminosity relations. Uncontracted or expanded haloes are required (Dutton et al. 2007, 2011).

Two main mechanisms have been shown to cause expansion: supernova (SN) feedback (Navarro, Eke & FrenkNavarro et al. 1996a; Mo & Mao 2004; Read & Gilmore 2005; Mashchenko, Couchman & Wadsley 2006; Pontzen & Governato 2012) and dynamical friction (El-Zant, Shlosman & Hoffman 2001; Tonini, Lapi & Salucci 2006; Romano-Díaz et al. 2008; Goerdt et al. 2010; Cole, Dehnen & Wilkinson 2011). SN feedback drives sufficient gas outflows to flatten the central DM density profile in simulated dwarf galaxies (Governato et al. 2010; Teyssier et al. 2013) into a 'core'. Dynamical friction smoothes DM density profiles during mergers.

The analytical model of Pontzen & Governato (2012) predicts that repeated outflows, rather than a single, impulsive mass-loss (as in Navarro, Eke & FrenkNavarro et al. 1996a), transfer energy to the DM. The rapid oscillations of the central gravitational potential perturb the DM orbits, creating a core. Mashchenko et al. (2006) described a similar mechanism in which SN-driven outflows changed the position of the halo centre, also creating a core. Macciò et al. (2012a) showed that reasonable amounts of feedback in fully cosmological simulations can result in DM cores rather than cusps in galaxies as massive as L^*. Governato et al. (2012) measured the inner DM slope in a sample of simulated dwarf galaxies, which matches well the stellar-to-halo mass ratio (Munshi et al. 2013), using a power-law density profile $\rho \propto r^\alpha$. They found that the slope α increases, i.e. the profile flattens, with increasing stellar mass.

In this paper, we study DM density profiles in a suite of galaxies drawn from the McMaster Unbiased Galaxy Simulations (MUGS, Stinson et al. 2010) and MaGICC projects (Brook et al. 2012; Stinson et al. 2013). The galaxies cover a broad mass range from dwarf to massive discs, and are simulated using a variety of stellar feedback implementations. The wide mass range of our simulated galaxies, $5.0 \times 10^5 < M_*/M_\odot < 8.3 \times 10^{10}$, allows us to confirm and extend the results of Governato et al. (2012). We show that the most relevant property for the determination of the DM inner slope is actually the stellar-to-halo mass ratio, i.e. the star formation efficiency, and that the relation between α and stellar mass turns over

such that the inner density profiles of more massive disc galaxies become increasingly steep.

We present our simulations in Section 2, the results and predictions in Section 3, and the conclusions in Section 4.

2 SIMULATIONS

The simulations used in this study are taken from the MUGS (Stinson et al. 2010), which is a sample of 16 zoomed-in regions where $\sim L^*$ galaxies form in a cosmological volume 68 Mpc on a side. MUGS uses a ΛCDM cosmology with $H_0 = 73$ km s^{-1} Mpc^{-1}, $\Omega_m = 0.24$, $\Omega_\Lambda = 0.76$, $\Omega_b = 0.04$ and $\sigma_8 = 0.76$ (*WMAP3*, Spergel et al. 2007).

All of the simulations are listed in Table 1 where they are separated into three mass groups: high, medium and low mass. The symbol shapes denote simulations with the same initial conditions, while the colours indicate the specific star formation and feedback model used. The medium- and low-mass initial conditions are scaled-down variants of the high-mass initial conditions, so that rather than residing in a 68 Mpc cube, they lie within a cube with 34 Mpc on a side (medium mass) or 17 Mpc on a side (low mass). This rescaling allows us to compare galaxies with exactly the same merger histories at three different masses. Differences in the underlying power spectrum that result from this rescaling are minor (Macciò et al. 2008; Springel et al. 2008; Kannan et al. 2012). Moreover, as shown through the paper, this methodology does not affect our analysis and results since we reach, at the low-halo-mass end where we have made the rescaling, the same conclusions as in Governato et al. (2012) whose galaxies do not have rescaled initial conditions.

Our galaxies were simulated using GASOLINE (Wadsley, Stadel & Quinn 2004), a fully parallel, gravitational N-body + smoothed particle hydrodynamics (SPH) code. Cooling via hydrogen, helium and various metal lines in a uniform ultraviolet ionizing background is included as described in Shen, Wadsley & Stinson (2010).

In addition to the hydrodynamic simulations, collisionless, DM-only simulations were performed for each initial condition. These DM-only runs exhibit a wide range of concentrations, from those typical of the L^* galaxies to those typical of the dwarf galaxies. The concentration, c, varies in the range $10 \lesssim c \lesssim 15$, where $c \equiv R_{vir}/r_s$ and r_s is the scale radius of the Navarro–Frenk–White (NFW) profile (Navarro et al. 1996b). Such a range is sufficient to study density profiles. Indeed, the sample includes a number of galaxies with high c at each mass range, a legacy of preferentially simulating galaxies with early formation times in order to model Milky Way formation.

The main haloes in our simulations were identified using the MPI+OpenMP hybrid halo finder AHF[1] (Gill, Knebe & Gibson 2004; Knollmann & Knebe 2009). AHF locates local overdensities in an adaptively smoothed density field as prospective halo centres. For a discussion of its performance with respect to simulations including baryonic physics, we refer the reader to Knebe et al. (2013). The virial masses of the haloes, M_{halo}, are defined as the masses within a sphere containing $\Delta = 390$ times the cosmic background matter density at $z = 0$.

2.1 Star formation and feedback

The hydrodynamic simulations all include star formation, with the stars feeding energy back into the interstellar medium (ISM) gas.

---

[1] http://popia.ft.uam.es/AMIGA

Table 1. Simulation parameters.

	MUGS label	Gas particle mass ($M_\odot$)	Softening length (pc)	$M_{\rm halo}$ ($M_\odot$)	$R_{\rm vir}$ (kpc)	M_* ($M_\odot$)	$E_{\rm SN}$	$\epsilon_{\rm esf}$	IMF	$n_{\rm th}$ (cm^{-3})	Symbol
Low	g1536	3.1×10^3	78.1	9.4×10^9	61	7.2×10^5	1.0	0.1	C	9.3	●
	g1536	3.1×10^3	78.1	9.4×10^9	60	5.1×10^5	1.0	0.125	C	9.3	●
	g1536	3.1×10^3	78.1	9.4×10^9	61	5.0×10^5	1.0	0.175	C	9.3	●
	g1536	3.1×10^3	78.1	9.4×10^9	60	7.0×10^5	1.2	0.0	C	9.3	●
	g15784	3.1×10^3	78.1	1.9×10^{10}	77	8.9×10^6	1.0	0.1	C	9.3	▲
	g15784	3.1×10^3	78.1	1.9×10^{10}	79	7.4×10^8	0.4	0	K	0.1	▲
	g15784	3.1×10^3	78.1	1.9×10^{10}	79	8.4×10^6	1.0	0.125	C	9.3	▲
	g15784	3.1×10^3	78.1	1.8×10^{10}	75	6.0×10^6	1.0	0.175	C	9.3	▲
	g15784	3.1×10^3	78.1	1.8×10^{10}	75	1.1×10^7	1.2	0.0	C	9.3	▲
	g15807	3.1×10^3	78.1	3.0×10^{10}	89	1.6×10^7	1.0	0.1	C	9.3	■
Medium	g7124	2.5×10^4	156.2	5.3×10^{10}	107	1.3×10^8	1.0	0.1	C	9.3	✳
	g5664	2.5×10^4	156.2	6.3×10^{10}	114	2.4×10^8	1.0	0.1	C	9.3	◆
	g5664	2.5×10^4	156.2	6.6×10^{10}	116	1.0×10^9	0.8	0.05	C	9.3	◆
	g5664	2.5×10^4	156.2	7.3×10^{10}	120	8.7×10^9	0.4	0	K	0.1	◆
	g1536	2.5×10^4	156.2	8.3×10^{10}	125	4.5×10^8	1.0	0.1	C	9.3	●
	g21647	2.5×10^4	156.2	9.6×10^{10}	131	2.0×10^8	1.0	0.1	C	9.3	◀
	g15784	2.5×10^4	156.2	1.8×10^{11}	161	4.3×10^9	1.0	0.1	C	9.3	▲
	g15784	2.5×10^4	156.2	1.8×10^{11}	161	2.4×10^9	1.0	0.125	C	9.3	▲
	g15784	2.5×10^4	156.2	1.9×10^{11}	164	7.1×10^9	1.0	0.1	K	9.3	▲
	g15784	2.5×10^4	156.2	1.7×10^{11}	157	8.6×10^8	1.0	0.1	C	9.3	▲
	g15807	2.5×10^4	156.2	2.9×10^{11}	189	1.5×10^{10}	1.0	0.1	C	9.3	■
High	g7124	2×10^5	312.5	4.5×10^{11}	219	6.3×10^9	1.0	0.1	C	9.3	✳
	g7124	2×10^5	312.5	4.9×10^{11}	227	5.1×10^{10}	0.4	0	K	0.1	✳
	g5664	2×10^5	312.5	5.6×10^{11}	236	2.7×10^{10}	1.0	0.1	C	9.3	◆
	g5664	2×10^5	312.5	5.7×10^{11}	237	4.9×10^{10}	0.4	0	K	0.1	◆
	g5664	2×10^5	312.5	5.9×10^{11}	241	1.4×10^{10}	1.0	0.175	C	9.3	◆
	g1536	2×10^5	312.5	7.2×10^{11}	257	2.4×10^{10}	1.0	0.1	C	9.3	●
	g1536	2×10^5	312.5	7.7×10^{11}	264	8.3×10^{10}	0.4	0	K	0.1	●
	g1536	2×10^5	312.5	7.0×10^{11}	254	1.1×10^{10}	1.0	0.125	C	9.3	●
	g1536	2×10^5	312.5	7.8×10^{11}	265	2.5×10^{10}	1.0	0.175	C	9.3	●
	g1536	2×10^5	312.5	7.0×10^{11}	255	1.8×10^{10}	1.2	0.0	C	9.3	●

A range of star formation and feedback parameters are used in this study: all of them employ blastwave SN feedback (Stinson et al. 2006), and some also include 'early stellar feedback', the energy that massive stars release prior to their explosions as SNe (Stinson et al. 2013).

In all simulations, gas is eligible to form stars when it reaches temperatures below 15 000 K in a dense environment, $n > n_{\rm th}$. Two different density thresholds are used for star formation, $n_{\rm th} = 0.1$ and 9.3 cm^{-3}. Gas denser than $n_{\rm th}$ is converted to stars according to the Kennicutt–Schmidt law (Kennicutt 1998):

$$\frac{\Delta M_*}{\Delta t} = c_* \frac{m_{\rm gas}}{t_{\rm dyn}}, \tag{1}$$

where ΔM_* is the mass of the stars formed in Δt, the time between star formation events (0.8 Myr in these simulations), $m_{\rm gas}$ is the mass of the gas particle, $t_{\rm dyn}$ is the gas particle's dynamical time and c_* is the fraction of gas that will be converted into stars during $t_{\rm dyn}$.

SN feedback is implemented using the Stinson et al. (2006) blastwave formalism, depositing $E_{\rm SN} \times 10^{51}$ erg into the surrounding ISM at the end of the lifetime of stars more massive than 8 $M_\odot$. Since stars form from dense gas, this energy would be quickly radiated away due to the efficient cooling. For this reason, cooling is disabled for particles inside the blast region. Metals are ejected from Type II SNe (SNeII), SNeIa and the stellar winds driven from asymptotic giant branch stars, and distributed to the nearest gas particles using the smoothing kernel (Stinson et al. 2006). The metals can diffuse between gas particles as described in Shen et al. (2010).

Early stellar feedback is included in most of our simulations. It uses a fraction, $\epsilon_{\rm esf}$, of the total luminosity emitted by massive stars. The luminosity of stars is modelled with a simple fit of the mass–luminosity relationship observed in binary systems (Torres 2010):

$$\frac{L}{L_\odot} = \begin{cases} (M/M_\odot)^4, & M < 10\,M_\odot \\ 100\,(M/M_\odot)^2, & M > 10\,M_\odot \end{cases} \tag{2}$$

Typically, this model corresponds to the emission of 2×10^{50} erg $M_\odot^{-1}$ of the entire stellar population over the $\sim$4.5 Myr between a star's formation and the commencement of SNeII in the region. These photons do not couple efficiently with the surrounding ISM (Freyer, Hensler & Yorke 2006). To mimic this highly inefficient energy coupling, we inject $\epsilon_{\rm esf}$ of the energy as thermal energy in the surrounding gas, and cooling is *not* turned off. Such thermal energy injection is highly inefficient at the spatial and temporal resolution of cosmological simulations (Katz 1992; Kay et al. 2002), as the characteristic cooling time-scales in the star-forming regions are lower than the dynamical time. In the fiducial model used in the MaGICC simulations, $\epsilon_{\rm esf} = 0.1$, which corresponds to the fraction of ionizing ultraviolet flux emitted from young stellar populations.

Two initial mass functions (IMFs) were used in the simulations. MUGS used a Kroupa, Tout & Gilmore (1993) IMF (denoted by K), while most of the rest used a Chabrier (2003) IMF (denoted by

C). Chabrier (2003) produces two times more SNeII per mass of stars born.

The fiducial feedback (red coloured symbols) includes early stellar feedback with $\epsilon_{esf} = 0.1$, 10^{51} erg of energy deposited per SN and a Chabrier (2003) IMF. The early stellar feedback efficiency ϵ_{esf} is increased from 0.1 to 0.125 (blue) in some simulations, while in others $\epsilon_{esf} = 0$, but the energy per SN is then increased by 20 per cent (cyan). In yellow, we include simulations with $\epsilon_{esf} = 0.175$, in which diffusion of thermal energy from gas particles (Wadsley, Veeravalli & Couchman 2008; Stinson et al. 2012) is allowed to occur during the adiabatic expansion phase. We also include simulations made with the original MUGS feedback, with 4×10^{50} erg per SN, a Kroupa et al. (1993) IMF and no ϵ_{esf}, which systematically overproduce the number of stars at each halo mass (black). Finally, an intermediate feedback implementation with $\epsilon_{esf} = 0.05$, a Chabrier IMF and 8×10^{50} erg per SN has been also added (purple).

The reader is referred to Stinson et al. (2013) for a study of the effects of the parameters on the galaxy properties. Suffice to say that the fiducial simulations best match present observed galaxy properties (see also Brook et al. 2012).

3 RESULTS

We study the response of the DM distribution to different feedback schemes within this full set of simulated galaxies. Some example density profiles are shown in Fig. 1. It shows how the DM density profiles of the hydrodynamic simulations can vary depending on physics (MUGS in black compared to MaGICC fiducial simulations, which use early stellar feedback, in red), galaxy mass (solid line at high mass and dashed line at medium mass), and how the hydrodynamic simulations compare with the DM-only run (solid grey line).

The halo profiles are calculated using logarithmically spaced bins and the DM central density is subsequently fitted using a single power law, $\rho \propto r^\alpha$, over a limited radial range. The vertical dashed lines in Fig. 1 show the fiducial range over which α is measured, $0.01 < r/R_{vir} < 0.02$, where R_{vir} is the virial radius. Other radial ranges are also used to ensure the robustness of our results.

The choice of $0.01R_{vir}$ as the inner most bin satisfies the Power et al. (2003) criterion for convergence even in our least resolved
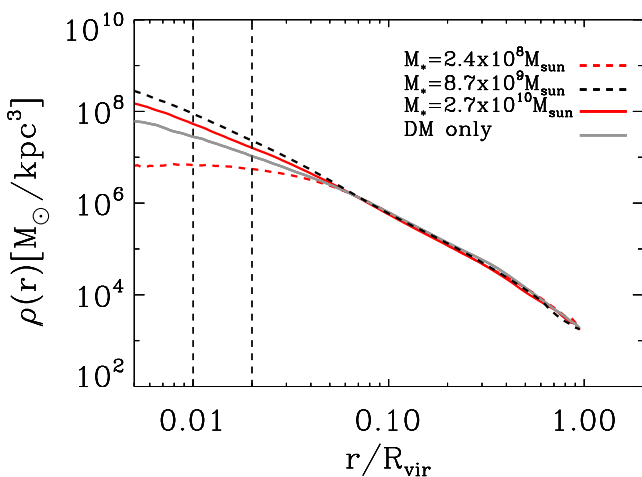
galaxy, as it encloses enough DM particles to ensure that the collisional relaxation time is longer than the Hubble time. This range is also straightforward to reproduce, and is not dependent on the resolution of the simulations. We also measured α in the range $3 < r/\epsilon < 10$, where ϵ is the softening length of each galaxy, and at a fixed physical range, $1 < r/\mathrm{kpc} < 2$. The choice of radial fitting range does not affect our results qualitatively, and only makes small quantitative differences which we show in our main results.

3.1 Inner slope as a function of halo mass

We first examine how α varies with stellar and halo mass. The top panel of Fig. 2 shows the M_*–M_{halo} relation for the entire suite of galaxies with the abundance matching prediction from Moster et al. (2013) indicated as the central solid black line with the 1σ uncertainties plotted as thin lines above and below the central relationship. Each galaxy is coloured according to the feedback model and symbol coded correspondingly to which initial condition was used, as described in Table 1.

Simulations are scattered around the M_*–M_{halo} relation. The fiducial feedback (red) represents the best fit to the abundance matching relation at every halo mass. Increasing the early stellar feedback efficiency ϵ_{esf} (blue) reduces the stellar mass by a factor of 2 at the high-mass end, while leaving the total number of stars relatively unchanged at the low-mass end, compared to the fiducial feedback.
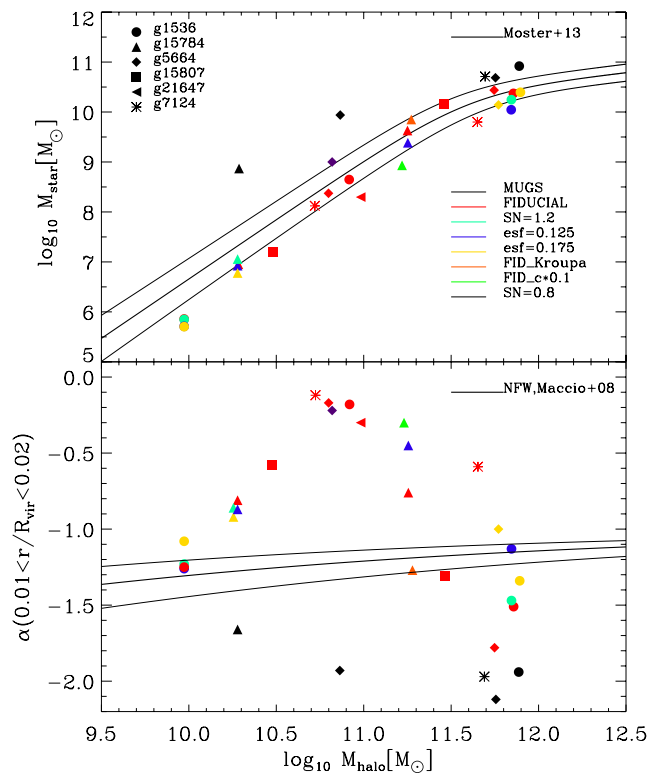
Figure 2. Top panel: the abundance matching relation for our suite of simulated galaxies. The feedback schemes are indicated with different colours, while the different galaxies are represented with symbols. The thick solid line corresponds to the abundance matching prediction from Moster, Naab & White (2013) and the thin lines are the 1σ uncertainty on it. Bottom panel: the inner slope of the DM distribution, measured between 0.01 and 0.02 of each galaxy's virial radius, as a function of the total halo mass. The solid lines are the theoretical expectation for DM haloes from Macciò et al. (2008) with its scatter.


Figure 1. Density profiles of contracted (solid red and dashed black lines) and expanded (dashed red line) DM haloes, together with the corresponding DM-only prediction (solid grey). The vertical dashed lines indicate 0.01 and 0.02 of the virial radius, our fiducial range to measure α.

When early stellar feedback is not included, the energy per SN must be increased to $E_{SN} = 1.2$ in order to lower the stellar mass to the Moster et al. (2013) relation (cyan). We note that the star formation history using such feedback is quite different from the fiducial runs, with more star formation at high redshift (see Stinson et al. 2013, for details). The yellow simulations that include high ϵ_{esf} have systematically lower stellar-to-halo mass ratios, and also have high late time star formation. Finally, the original MUGS feedback (black) systematically forms too many stars at each halo mass.

The bottom panel of Fig. 2 shows α as a function of halo mass, where M_{halo} comes from the full hydrodynamical simulation.[2] The solid black line shows the theoretical expectation of α as a function of halo mass for the DM-only case, as in Macciò et al. (2008) assuming a *WMAP3* cosmology; the thin solid lines represent the scatter in the c–M_{halo} relation.

At fixed halo mass, α varies greatly, depending on the feedback strength. The simulations that most closely follow the M_*–M_{halo} relationship show a notable flattening of inner profile slopes as mass increases, as in Governato et al. (2012). This flattening is due to the increasing energy available from SN explosions, as derived in Peñarrubia et al. (2012). Indeed, all the galaxies in our sample whose inner slope is shallower than the corresponding DM run have had an energy injection from SNe equal to or higher than the conservative values found in Peñarrubia et al. (2012). We note, however, that in our simulations the core-creation process does not only depend on the total amount of energy available: in the g15784 MUGS dwarf galaxy (black triangle), for example, the energy from SNe is higher than in the g15784 dwarfs of the same mass that had an expansion, yet this galaxy is strongly contracted. What we observe is the interplay between the energy from stellar feedback and the increased potential well caused by the high number of stars at the galaxy centre (see the next section for more details).

The profiles are flattest around $M_{halo} \sim 10^{11}$ M$_\odot$.

At higher masses, however, the inner profiles steepen again. All the simulations above the M_*–M_{halo} relationship have inner slopes $\alpha < -1.5$, i.e. a contracted halo steeper than the DM expectation at each halo mass. These simulations are all black coloured indicating that they were part of the MUGS simulations.

Thus, depending on the feedback and the halo mass used, the DM haloes may expand, contract or retain the initial NFW inner slope. It seems that the inner slope of the DM density profile does not show a clear dependence on halo mass (or equivalently stellar mass) when different feedback schemes are included.

3.2 Inner slope as a function of the stellar-to-halo mass ratio

While there is not a well-defined relation between α and stellar or halo mass individually, Fig. 3 shows α, measured in the range $0.01 < r/R_{vir} < 0.02$, plotted as a function of M_*/M_{halo}. The DM inner profile slope shows a tight relationship as a function of M_*/M_{halo}: indeed, much of the scatter apparent when α was plotted as a function of M_{halo} disappears. The grey area indicates the region where the M_*/M_{halo} ratios are more than 1σ above the M_*/M_{halo} peak in the abundance matching relation. Real galaxies do not have these star formation efficiencies.

The tight relationship between α and M_*/M_{halo} points to the conditions in which stellar feedback can create DM density cores.
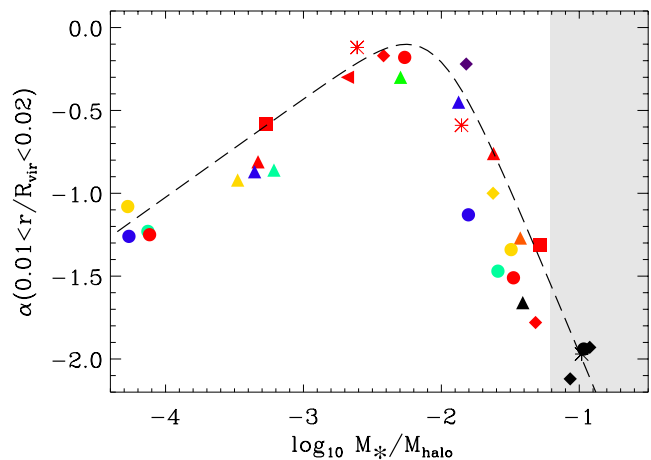
Figure 3. The relation between the DM density profile slope, α, measured in the range $0.01 < r/R_{vir} < 0.02$, and the stellar-to-halo-mass ratio of each galaxy. The colours and symbols are the same as in Fig. 2. The best-fitting function of equation (3) is overplotted as a dashed line. The grey area on the right-hand side indicates the 1σ peak in the M_*/M_{halo} abundance matching.

At low values of M_*/M_{halo}, the stellar content per halo mass is too small for the feedback energy to modify the DM distribution, and the halo of such galaxies retains a cuspy profile. As the stellar content per halo mass increases, the feedback energy is strong enough to produce expanded DM haloes, and thus for increasing values of M_*/M_{halo} the inner slope of DM profiles gets flatter, reaching a maximum of $\alpha = -0.10$ at $M_*/M_{halo} = 0.5$ per cent. The maximum value of α is even smaller, i.e. the profiles are flatter, if the inner slope is measured closer to the centre. At $3 < r/\epsilon < 10$, $\alpha \sim 0$ at $M_*/M_{halo} = 0.35$ per cent. At higher masses, the number of stars formed in the central regions deepens the potential well at the centre of the galaxies, opposing the expansion process and leading to increasingly cuspy profiles for higher values of M_*/M_{halo}.

We verified this claim by studying in detail the medium mass version of g15784 for different choices of feedback parameters. We found that the stellar mass within 1 kpc is a good indicator of the minimum of the potential in each galaxy and that, as expected, the medium mass, cored most version of g15784 (green triangle) has the shallowest potential well. Looking at the evolution of this galaxy, we observe that its star formation rate (SFR) decreases with time and correspondingly the M_*/M_{halo} value within 1 kpc is fairly constant at every redshift, reaching only 0.1 at $z = 0$; the fraction of gas versus stars at the centre is always very high, making possible the core creation since there is enough gas per total mass (or stellar mass) to be efficient in flattening the profile.

This process does not occur in the cuspy version g15784 fiducial (red triangle), which has a constant SFR after 11 Gyr and its M_*/M_{halo} ratio within 1 kpc increases up to 0.4 at $z = 0$: the increasing number of stars at the centre causes the gas versus stars ratio to become very low; therefore, the gas available for the outflows is not sufficient to be effective at flattening the profile because the potential well has been deepened by the stars.

We note that the total amount of gas in the inner 1kpc is similar in both the cored and the cuspy medium mass versions of g15784: it is not the absolute amount of gas which regulates the cusp–core transition, but its relative value compared to the total (or stellar) inner mass. We conclude that stellar mass at the galaxy centre and in particular the ratio M_*/M_{halo} is the most important quantity at indicating the deepening of the gravitational potential which balances the energy released from SNe.

---

[2] Using M_{halo} taken from the DM-only run provides similar results, as the halo mass amongst DM and SPH simulations changes by only a few per cent.

The relationship shown in Fig. 3 can be analytically modelled. We use a four-parameter, double-power-law function, whose best fit is shown in Fig. 3 as a dashed black line:

$$\alpha(X) = n - \log_{10}\left[\left(\frac{X}{x_0}\right)^{-\beta} + \left(\frac{X}{x_0}\right)^{\gamma} \right], \tag{3}$$

where $X = M_*/M_{\rm halo}$ while β and γ are the low and high star forming efficiency slopes. The best-fitting parameters, summarized in Table 2, were obtained using a χ^2 minimization fitting analysis. The same dependence, but with a different normalization, is obtained for the various criteria used to define the inner radial range, also shown in Table 2.

Fig. 4 shows the abundance matching relationship of $M_*/M_{\rm halo}$ as a function of $M_{\rm halo}$ colour coded according to the expected value of the DM inner slope when α is measured at $0.01 < r/R_{\rm vir} < 0.02$. The halo mass at which the flattest DM profiles are expected to be found, corresponding to a peak $M_*/M_{\rm halo} = 0.5$ per cent, is $M_{\rm halo} \approx 10^{10.8}$ M$_\odot$. The profile becomes increasingly cuspy, approaching the NFW value for galaxies near the Milky Way mass: only galaxies with $M_*/M_{\rm halo} > 3.8$ per cent, which is the peak in the abundance matching prediction, are contracted. Such galaxies are outliers in the Universe.

3.3 Core creation

We next examine which mechanism is responsible for the creation of cores, using the three simulations shown in Fig. 1 as case studies. As outlined in Section 1, core formation from stellar feedback depends on repeated starbursts that are able to move gas enough to have a

Table 2. Best-fitting parameters and relative errors for the α versus $M_*/M_{\rm halo}$ relation. The reduced chi-square is also listed.

Radial range	n	$\log_{10}x_0$	β	γ	χ_r^2
$0.01 < r/R_{\rm vir} < 0.02$	0.132	−2.051	0.593	1.99	1.16
	±0.042	±0.074	±0.086	±0.32	
$1 < r/{\rm kpc} < 2$	0.168	−2.142	0.699	1.56	1.29
	±0.031	±0.133	±0.213	±0.12	
$3 < r/\epsilon < 10$	0.231	−2.209	0.494	1.49	1.28
	±0.043	±0.064	±0.055	±0.55	

Figure 4. The abundance matching prediction colour coded according to the expected value of the DM inner slope at every halo mass. We used the best-fitting parameters of α measured between 0.01 and 0.02 of each galaxy's virial radius.

dynamical effect on the DM (Read & Gilmore 2005; Governato et al. 2010; Macciò et al. 2012a; Pontzen & Governato 2012; Teyssier et al. 2013).

The four panels of Fig. 5 show how some relevant quantities vary as a function of look-back time. From the top to bottom we present: (i) the star formation history, which shows clear starbursts that can drive outflows; (ii) the gas mass within a sphere of 1 kpc from the centre of the galaxy, which shows when the gas has been driven out of the galaxy centre; (iii) the distance Δ between the position of the DM and gas potential minima, which shows how much the baryonic centre of mass moves around; and (iv) the $M_*/M_{\rm halo}$ value that determines α.
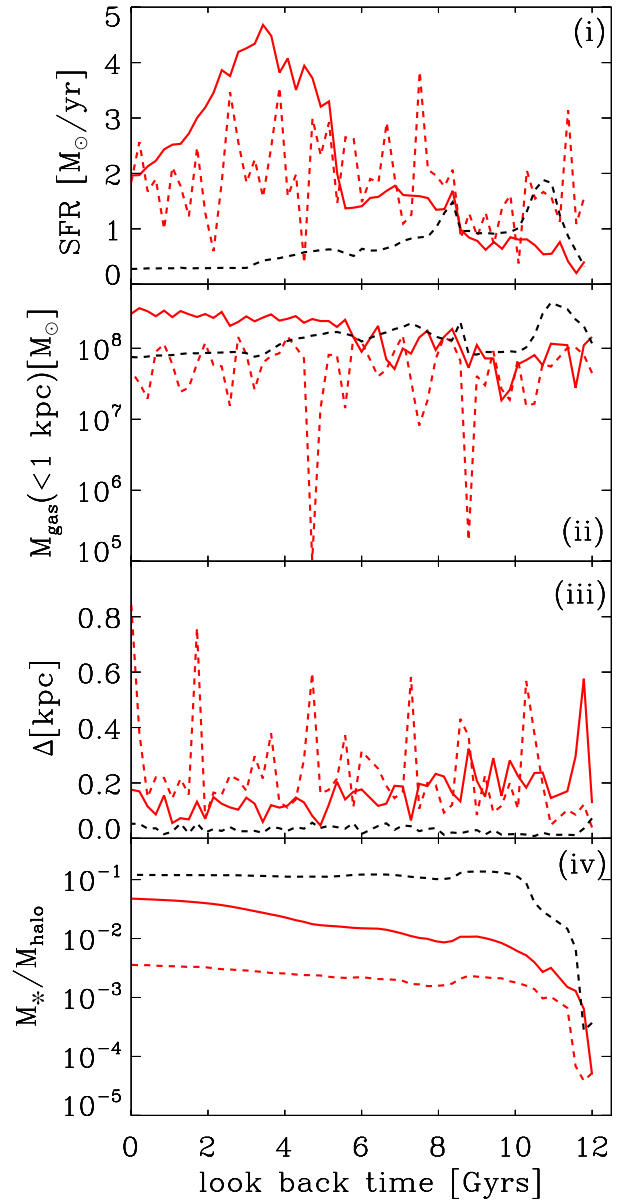
Figure 5. For the galaxies in Fig. 1, we show the evolution of (i) the star formation history; (ii) the gas flows within a 1 kpc sphere centred at the galaxy centre; (iii) the relative position between gas and DM potential minima; and (iv) $M_*/M_{\rm halo}$ as a function of look-back time. Note that the SFR of the $M_* = 2.4 \times 10^8$ M$_\odot$ galaxy (red dashed line) has been multiplied by a factor 100 in order to be shown in the same scale range.

The medium mass version of g5664 that uses the fiducial MaGICC feedback (red dashed line) has the flattest density profile at $z = 0$, so we expect it to have the most violent history. Indeed, it has a bursty star formation history (multiplied by 100 to get it into the same range as the other galaxy star formation histories), and a star formation efficiency, M_*/M_{halo}, that stays near the optimal value for cores, between ~0.35 and 0.5 per cent throughout its evolution. A couple of the bursts of star formation cause significant gas loss from the inner 1 kpc, which results in consistent offsets between the positions of the centre of gas and DM distributions.

The medium mass version of g5664 that uses the low-feedback MUGS physics (dashed black line) is the most contracted galaxy of this set. Other than a peak of SFR at an early time, corresponding to its peak DM accretion, its star formation history is a smoothly declining exponential. This early star formation quickly drives the efficiency M_*/M_{halo} to values higher than 10 per cent, which, according to Fig. 3, leads to a cuspy density profile. The high number of stars already formed 11 Gyr ago within this galaxy create a deep potential well which suppresses the effects of stellar feedback, so that little gas flows out of the inner regions, and the DM and gas distributions share the same centre of mass throughout the galaxy's evolution.

Perhaps the most interesting case is that of the fiducial high-mass g5664 galaxy (red solid line). At $z = 0$ its DM profile is slightly contracted compared to the NFW halo, but less contracted than the lower mass MUGS case (dashed black line). Indeed, its star formation efficiency, $M_*/M_{halo} \sim 5$ per cent at $z = 0$, is lower than the MUGS case, but still high enough to have contracted DM. This galaxy shows elevated star formation starting ~6 Gyr ago, which correlates with an increase of M_*/M_{halo}, increased gas in the centre with fewer outflows and a more constant Δ. Before $z = 0.66$ the star formation efficiency, M_*/M_{halo}, of this galaxy was still ~1 per cent, and the feedback energy was still able to cause gas flows and variations in Δ. When we examine the galaxy at that epoch, it indeed had an expanded DM profile with $\alpha > -1.0$, measured between 0.01 and 0.02 of the physical virial radius. Immediately after the starburst the star formation efficiency increases, the DM and gas start to share the same centre, the outflows from the inner region diminish, and the profile steepens to $\alpha < -1.0$ by $z = 0.66$ (6 Gyr ago) and finally to $\alpha = -1.8$ by $z = 0$ with a star formation efficiency of $M_*/M_{halo} \sim 5$ per cent.

3.4 Predictions for observed galaxies

Combining the parameters in Table 2 with the Moster et al. (2013) relationship, it is possible to predict the inner density profile slope of a galaxy based on its observed stellar mass. This allows us to make predictions which are independent of the feedback prescription. Using the best-fitting parameters from the $0.01 < r/R_{vir} < 0.02$ range, we can compute the median expected α dependence on stellar mass for galaxies as massive as $M_{halo} \approx 10^{12}$ M$_\odot$ ($M_* \approx 3.4 \times 10^{10}$ M$_\odot$):

$$\alpha = 0.132 - \log_{10}\left[\frac{\eta^{2.58} + 1}{\eta^{1.99}}\right], \tag{4}$$

where

$$\eta = 0.84\left(\frac{M_*}{10^9 M_\odot}\right)^{-0.58} + 0.06\left(\frac{M_*}{10^9 M_\odot}\right)^{0.26}. \tag{5}$$

The peak of this function occurs at $M_* = 10^{8.5}$ M$_\odot$ and the low-mass-end slope, 0.34, is in good agreement with the one obtained in Governato et al. (2012) for stellar masses in the range

$10^4 < M_*/$M$_\odot < 10^{9.4}$. Our study extends the prediction of cores versus cusps to L* scales and predicts a turnover in the relation between inner slope and galaxy mass for $M_* > 10^{8.5}$ M$_\odot$: above this value, the inner slope decreases as $\alpha \propto -0.64\log_{10}M_*/M_\odot$.

Taking a step further, the stellar content of galaxies is then connected to their observed rotation velocity through the Tully–Fisher (TF) relation. Equation (4) of Dutton et al. (2010) parametrizes V_{rot} at 2.2 I-band exponential scalelengths as a function of M_*. Using this M_*–V_{rot} relation we predict α as a function of V_{rot}, the rotation velocity of galaxies. Fig. 6 shows, for the different radial ranges where we measure the inner density profile, α as a function of observed rotation velocity for galaxies with $M_{halo} \leq 10^{12}$ M$_\odot$. The dashed lines indicate where the TF relationship was linearly extrapolated for $M_* < 10^9$ M$_\odot$.

Fig. 6 shows that the galaxies with the flattest inner density profiles are found at $V_{rot} \sim 50$ km s^{-1}. α decreases in more massive galaxies where the inner density profiles become more cuspy until they reach the NFW profile.

We note that the position at which the inner slope is measured has an effect on the α values, which alters the best-fitting parameters reported in Table 2, and consequently determines how α varies with rotation velocity. Thus, Fig. 6 has to be interpreted according to the radial range chosen, though the general trends are not changed and the peak of α remains at $V_{rot} \sim 50$ km s^{-1}, independent of where the slope is measured.

The major difference between α measured at $0.01 < r/R_{vir} < 0.02$ and the other radial ranges is that the inner slope is steeper for $V_{rot} > 100$ km s^{-1} in the former case. A steeper slope is expected because $0.01 < r/R_{vir} < 0.02$ is farther from the galaxy centre than the other two measurements. However, none of the measured α values falls below the NFW expectation as V_{rot} approaches 250 km s^{-1}. Thus, DM haloes are never contracted in our model, even in the most massive disc galaxies.

4 CONCLUSIONS

Using 31 simulated galaxies from the MaGICC project, we showed that DM density profiles are modified by baryonic processes in the centre of galactic haloes. The inner profile slope depends solely on the mass of stars formed per halo mass and is independent of the particular choice of feedback parameters within our blastwave and early stellar feedback scheme. Similar to previous work, the
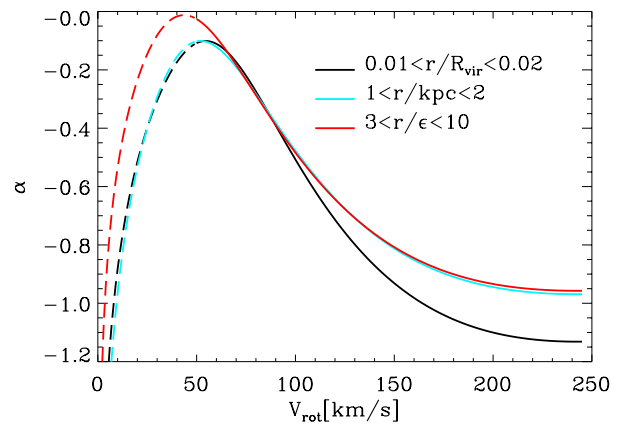
Figure 6. Expected relation between the galaxies' rotation velocity and inner slope of their DM haloes. The three lines correspond to different radial ranges used for measuring α. The dashed lines refer to the linear extrapolation of the baryonic TF relation (Dutton et al. 2010) below $M_* = 10^9$ M$_\odot$.

expansion of the DM profile results from SN-driven outflows that cause fluctuations in the global potential and shift the centre of the gas mass away from the centre of the DM mass.

At values of $M_*/M_{halo} \lesssim 0.01$ per cent, the energy from stellar feedback is not sufficient to modify the DM distribution, and these galaxies retain a cuspy profile. At higher stellar-to-halo mass ratios, feedback drives the expansion of the DM haloes, resulting in cored profiles. The shallowest profiles form in galaxies with $M_*/M_{halo} \sim 0.5$ per cent. According to the abundance matching relation (Moster et al. 2013), these galaxies have $M_{halo} \approx 10^{10.8}$ $M_{\odot}$ and $M_* \approx 10^{8.5}$ $M_{\odot}$. In higher mass haloes, the deepening of the potential due to stars that form in the central regions suppresses SN-driven outflows and thus lowers expansion, leaving cuspier profiles.

The abundance matching peak of star formation efficiency, $M_*/M_{halo} = 3.8$ per cent, occurs at $M_{halo} = 10^{11.76}$ $M_{\odot}$, which is close to the lowest current estimate of the Milky Way mass. Our model predicts that such a halo will be uncontracted and have an NFW-like inner slope of $\alpha = -1.20$ when the slope is measured between ~ 2 and ~ 4 kpc.

We combine our parametrization of α as a function of M_*/M_{halo} with the empirical abundance matching relation to assign a median relationship between α and M_*. The inner slope of the DM density profile increases with stellar mass to a maximum (most cored profile) at $M_* \approx 10^{8.5}$ $M_{\odot}$, before decreasing towards cuspier profiles at higher stellar masses. Below $M_* \approx 10^{8.5}$ $M_{\odot}$ the DM inner slope increases with stellar mass as $\alpha \propto 0.34 \log_{10} M_*/M_{\odot}$, similar to the relation found in Governato et al. (2012). For $M_* > 10^{8.5}$ $M_{\odot}$, DM haloes become cuspier, with $\alpha \propto -0.64 \log_{10} M_*/M_{\odot}$.

The TF relation allows us to predict the dependence of the DM inner slope on the observed rotation velocity of galaxies. Using our results and the stellar mass TF relation from Dutton et al. (2010), we find that the flattest inner profiles are expected for galaxies with $V_{rot} \sim 50$ km s^{-1}. α decreases for more massive galaxies, leading to cuspier profiles and eventually reaching the NFW prediction at the Milky Way mass. We note that, in agreement with our findings, the most clear observational measurements of flattened 'core' profiles of disc galaxies (de Blok et al. 2008; Kuzio de Naray et al. 2008, 2009; Oh et al. 2011) are found in low surface brightness galaxies with $V_{rot} < 100$ km s^{-1}.

More massive disc galaxies, being baryon dominated, suffer from larger uncertainties in the disc–halo decomposition of their rotation curves, making it difficult to distinguish if their DM profile is cuspy or cored. Some studies conclude that such galaxies, those with $V_{rot} > 150$ km s^{-1}, can be described with cored profiles (Borriello & Salucci 2001; Donato, Gentile & Salucci 2004; McGaugh et al. 2007), while others find that the NFW model provides equally good fits for these high-luminosity galaxies (de Blok et al. 2008; Kuzio de Naray et al. 2008).

More recently, Martinsson et al. (2013) presented rotation-curve mass decompositions of several massive spiral galaxies, and found no significant difference between the quality of a pseudo-isothermal sphere or an NFW model in fitting the DM rotation curves of individual galaxies, given the uncertainties in the contribution of baryons. If high surface brightness discs are submaximal (e.g. Courteau & Rix 1999), their haloes are allowed to be cuspy at the centre.

An aspect not taken into account in our simulations of galaxy formation is the influence of active galactic nucleus feedback on the density profile of DM haloes. We acknowledge that this form of feedback starts to be relevant at the high-halo-mass end, where we observe increasingly cuspy galaxies: the study of the core–cusp problem would thus benefit from a future implementation of this type of feedback.

Our novel prediction for cusp versus core formation can be tested and, at least at the low-halo-mass end, well constrained using observational data sets. This study can be applied to theoretical modelling of galaxy mass profiles, as well as to modelling of populations of disc galaxies within CDM haloes. We find this encouraging and hope that our study motivates more systematic analysis of the dependance of α on galaxy mass in real disc galaxies.

REFERENCES

Ade P. A. R. et al. (Planck Collaboration), 2013, preprint (arXiv:e-prints)
Avila-Reese V., Colín P., Valenzuela O., D'Onghia E., Firmani C., 2001, ApJ, 559, 516
Blumenthal G. R., Faber S. M., Primack J. R., Rees M. J., 1984, Nat, 311, 517
Blumenthal G. R., Faber S. M., Flores R., Primack J. R., 1986, ApJ, 301, 27
Bode P., Ostriker J. P., Turok N., 2001, ApJ, 556, 93
Borriello A., Salucci P., 2001, MNRAS, 323, 285
Brook C. B., Stinson G., Gibson B. K., Wadsley J., Quinn T., 2012, MNRAS, 424, 1275
Chabrier G., 2003, ApJ, 586, L133
Cole D. R., Dehnen W., Wilkinson M. I., 2011, MNRAS, 416, 1118
Courteau S., Rix H.-W., 1999, ApJ, 513, 561
de Blok W. J. G., Bosma A., McGaugh S., 2003, MNRAS, 340, 657
de Blok W. J. G., Walter F., Brinks E., Trachternach C., Oh S.-H., Kennicutt R. C., Jr, 2008, AJ, 136, 2648
Donato F., Gentile G., Salucci P., 2004, MNRAS, 353, L17
Dutton A. A., van den Bosch F. C., Dekel A., Courteau S., 2007, ApJ, 654, 27
Dutton A. A., Conroy C., van den Bosch F. C., Prada F., More S., 2010, MNRAS, 407, 2
Dutton A. A. et al., 2011, MNRAS, 416, 322
Einasto J., 1965, T. Inst. Astrofiz. Alma-Ata, 51, 87
El-Zant A., Shlosman I., Hoffman Y., 2001, ApJ, 560, 636
Freyer T., Hensler G., Yorke H. W., 2006, ApJ, 638, 262
Gill S. P. D., Knebe A., Gibson B. K., 2004, MNRAS, 351, 399

Gnedin O. Y., Kravtsov A. V., Klypin A. A., Nagai D., 2004, ApJ, 616, 16

Goerdt T., Moore B., Read J. I., Stadel J., 2010, ApJ, 725, 1707

Governato F. et al., 2010, Nat, 463, 203

Governato F. et al., 2012, MNRAS, 422, 1231

Graham A. W., Merritt D., Moore B., Diemand J., Terzić B., 2006, AJ, 132, 2701

Hinshaw G. et al., 2013, ApJS, 208, 19

Kannan R., Macciò A. V., Pasquali A., Moster B. P., Walter F., 2012, ApJ, 746, 10

Katz N., 1992, ApJ, 391, 502

Kay S. T., Pearce F. R., Frenk C. S., Jenkins A., 2002, MNRAS, 330, 113

Kennicutt R. C., 1998, ApJ, 498, 541

Knebe A., Devriendt J. E. G., Mahmood A., Silk J., 2002, MNRAS, 329, 813

Knebe A. et al., 2013, MNRAS, 435, 1618

Knollmann S. R., Knebe A., 2009, ApJS, 182, 608

Komatsu E. et al., 2011, ApJS, 192, 18

Kroupa P., Tout C. A., Gilmore G., 1993, MNRAS, 262, 545

Kuhlen M., Vogelsberger M., Angulo R., 2012, Phys. Dark Universe, 1, 50

Kuzio de Naray R., McGaugh S. S., de Blok W. J. G., 2008, ApJ, 676, 920

Kuzio de Naray R., McGaugh S. S., Mihos J. C., 2009, ApJ, 692, 1321

Macciò A. V., Dutton A. A., van den Bosch F. C., 2008, MNRAS, 391, 1940

Macciò A. V., Stinson G., Brook C. B., Wadsley J., Couchman H. M. P., Shen S., Gibson B. K., Quinn T., 2012a, ApJ, 744, L9

Macciò A. V., Paduroiu S., Anderhalden D., Schneider A., Moore B., 2012b, MNRAS, 424, 1105

McGaugh S. S., de Blok W. J. G., Schombert J. M., Kuzio de Naray R., Kim J. H., 2007, ApJ, 659, 149

Martinsson T. P. K., Verheijen M. A. W., Westfall K. B., Bershady M. A., Andersen D. R., Swaters R. A., 2013, A&A, 557, A131

Mashchenko S., Couchman H. M. P., Wadsley J., 2006, Nat, 442, 539

Mo H. J., Mao S., 2004, MNRAS, 353, 829

Moster B. P., Naab T., White S. D. M., 2013, MNRAS, 428, 3121

Munshi F. et al., 2013, ApJ, 766, 56

Navarro J. F., Eke V. R., Frenk C. S., 1996a, MNRAS, 283, L72

Navarro J. F., Frenk C. S., White S. D. M., 1996b, ApJ, 462, 563

Navarro J. F. et al., 2010, MNRAS, 402, 21

Oh S.-H., de Blok W. J. G., Brinks E., Walter F., Kennicutt R. C., Jr, 2011, AJ, 141, 193

Peñarrubia J., Pontzen A., Walker M. G., Koposov S. E., 2012, ApJ, 759, L42

Pontzen A., Governato F., 2012, MNRAS, 421, 3464

Power C., Knebe A., 2006, MNRAS, 370, 691

Power C., Navarro J. F., Jenkins A., Frenk C. S., White S. D. M., Springel V., Stadel J., Quinn T., 2003, MNRAS, 338, 14

Read J. I., Gilmore G., 2005, MNRAS, 356, 107

Riess A. G. et al., 1998, AJ, 116, 1009

Romano-Díaz E., Shlosman I., Hoffman Y., Heller C., 2008, ApJ, 685, L105

Salucci P., Burkert A., 2000, ApJ, 537, L9

Shen S., Wadsley J., Stinson G., 2010, MNRAS, 407, 1581

Simon J. D., Bolatto A. D., Leroy A., Blitz L., Gates E. L., 2005, ApJ, 621, 757

Spergel D. N. et al., 2007, ApJS, 170, 377

Springel V., 2005, MNRAS, 364, 1105

Springel V. et al., 2008, MNRAS, 391, 1685

Stinson G., Seth A., Katz N., Wadsley J., Governato F., Quinn T., 2006, MNRAS, 373, 1074

Stinson G. S., Bailin J., Couchman H., Wadsley J., Shen S., Nickerson S., Brook C., Quinn T., 2010, MNRAS, 408, 812

Stinson G. S. et al., 2012, MNRAS, 425, 1270

Stinson G. S., Brook C., Macciò A. V., Wadsley J., Quinn T. R., Couchman H. M. P., 2013, MNRAS, 428, 129

Swaters R. A., Madore B. F., van den Bosch F. C., Balcells M., 2003, ApJ, 583, 732

Teyssier R., Pontzen A., Dubois Y., Read J. I., 2013, MNRAS, 429, 3068

Tonini C., Lapi A., Salucci P., 2006, ApJ, 649, 591

Torres G., 2010, AJ, 140, 1158

Wadsley J. W., Stadel J., Quinn T., 2004, New Astron., 9, 137

Wadsley J. W., Veeravalli G., Couchman H. M. P., 2008, MNRAS, 387, 427

White S. D. M., Rees M. J., 1978, MNRAS, 183, 341

This paper has been typeset from a TₑX/LⁱaTₑX file prepared by the author.